Electrochemistry Communications 118 (2020) 106784

Contents lists available at ScienceDirect

Electrochemistry Communications

journal homepage: www.elsevier.com/locate/elecom

Influence of cyano substituents on the electron density and catalytic activity towards the oxygen reduction reaction for iron phthalocyanine. The case for Fe(II) 2,3,9,10,16,17,23,24-octa(cyano)phthalocyanine

Joseph Govan[a], Gabriel Abarca[b], Carolina Aliaga[c,d], Byran Sanhueza[c], Walter Orellana[e], Gloria Cárdenas-Jirón[c], José H. Zagal[c], Federico Tasca[c,*]

[a] Departamento de Ingeniería y Suelos, Facultad de Ciencias Agronómicas, Universidad de Chile, Santiago, Chile
[b] Universidad Bernardo O'Higgins, Escuela de Obstetricia y Puericultura, Centro Integrativo de Biología y Química Aplicada (CIBQA), Santiago 8370993, Chile
[c] Facultad de Química y Biología, Universidad de Santiago de Chile, Santiago, Chile
[d] Centro para el Desarrollo de la Nanociencia y la Nanotecnología, CEDENNA, Chile
[e] Departamento de Ciencias Físicas, Universidad Andres Bello, Sazié 2212, 837-0136 Santiago, Chile

ARTICLE INFO

Keywords:
Oxygen Reduction Reaction
Electrocatalysis
Volcano correlation
Cyano substituents
Phthalocyanines
Carbon nanotubes

ABSTRACT

Iron(II) 2,3,9,10,16,17,23,24-octa(cyano)phthalocyanine (OCNFePc), was tested as a catalyst for the oxygen reduction reaction (ORR) adsorbed on carbon nanotubes. The composite was analyzed spectroscopically and electrochemically characterized at pH 13 and pH 1. The composite showed close to 4 electron processes at pH 13. Computational analysis indicates that the O_2 molecule binds end-on to the metal center and that the di-oxygen molecule is dissociated on both the Fe metal center and the corral ring. An Analysis of the molecular electrostatic potential confirms the behavior of cyano residues as electron-withdrawing moieties in OCNFePc. As a result of its catalytic behavior and theoretical analysis of its O_2 binding energy, OCNFePc was placed in a high position on a volcano correlation of similar phthalocyanine composites.

1. Introduction

Four-coordinate metal macrocyclic complexes (MN4) have gained attention as model catalysts because of their accessibility, low cost, and stability [1–4]. These materials have been reported as catalysts for the oxygen reduction reaction (ORR) since 1964 [5]. One goal of their use is to replace expensive Pt-containing catalysts as the O_2 cathode for fuel cells [6]. MN4 catalysts can only compete with Pt in alkaline media [7], not acid [6]. This is due to H_2O_2 production [8], indicative of incomplete reduction of oxygen through two-electron processes being more likely in acid instead of the complete reduction of oxygen through four-electron processes. Understanding the properties that favor four-electron processes is important for intelligently designing new catalysts [1,8–12]. This involves the development and characterization of novel substituted macrocycle catalysts [1,13–15] with different properties. The most important of these properties are the O_2 binding energy and the redox potential of the complexes [12,16]. When plotting the logarithm of the catalytic activity of these catalysts as formulated as the logarithm of the current density at a constant potential versus O_2 binding energy or redox potentials a volcano-shaped plot is obtained [12]. Volcano correlations are an effective method to visualize the optimal catalytic activity resulting from compromise in the substrate-catalyst bonding energy, i.e. neither too weak nor too high; in the present catalyst family, the "ascending" volcano side corresponds to weaker binding catalysts, such as most CoN4 ones, and the "descending" side corresponds to stronger binding catalysts, such as FeN4 ones [12,17]. Strong O_2 binding means strong peroxide binding so peroxide intermediates remain at the active site, promoting the 4-electron process [12,17,18]. Previous work by the authors has shown that withdrawing electron density from the metal center through the use of chlorine [14,19], nitro [14], and fluorine [20] residues or a fifth axial ligand [21–26], increase O_2 binding energy altering ORR activity. In this context, the case for substitution with CN groups has not been investigated so far, in spite of the substituent's remarkable electron withdrawing effect, as a result of Hammett parameters significantly more positive than Cl or F substituents [27–30].

In this work, a new catalyst for the ORR, Iron(II) 2,3,9,10,16,17,23,24-octa(cyano)phthalocyanine (OCNFePc) with eight CN substituents was tested. MN4 complexes tend to pile because of molecular stacking, but form monolayers on CNT surface allowing high

* Corresponding author.
E-mail address: federico.tasca@usach.cl (F. Tasca).

https://doi.org/10.1016/j.elecom.2020.106784
Received 30 June 2020; Accepted 2 July 2020
Available online 08 July 2020

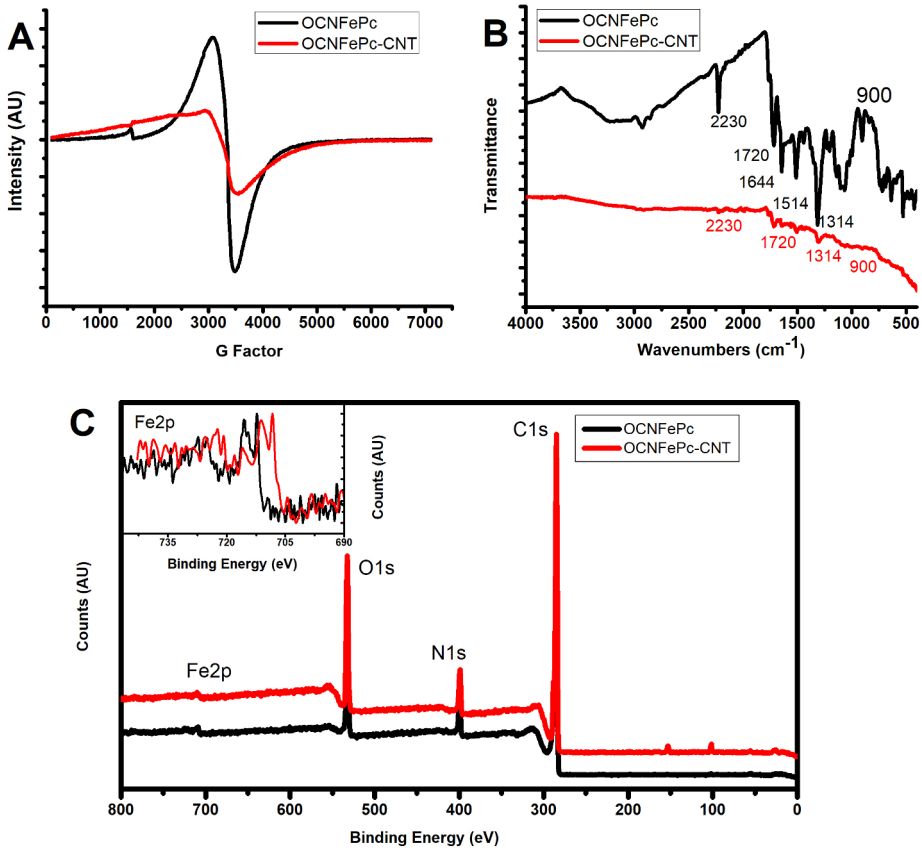

Fig. 1. Spectroscopic analysis of OCNFePc and OCNFePc-CNT. Showing EPR (A), FTIR (B) and XPS (C).

concentration of catalyst and high conductivity and therefore were used in this work. This material has already been reported for the synthesis of polymers [31,32] and metal organic frameworks [33] but has never been studied as a catalyst. FTIR, EPR and XPS spectroscopy was used to characterize this material. The O_2-Fe binding energies and electron withdrawing effect of the CN residues were calculated and used in conjunction with electrochemical characterization to determine its place in the volcano correlation.

2. Materials and methods

Fe(II) 2,3,9,10,16,17,23,24-octa(cyano)phthalocyanine phthalocyanine (OCNFePc) was obtained from PorphyChem (Dijon, France) and used as is. Isopropyl alcohol, NaOH, H_2SO_4 and Nafion™ were obtained from Sigma (St. Louis, USA). CNTs were obtained from Cheaptubes inc. (Grafton Vermont USA). The counter electrode was either a 0.1 cm diameter Pt wire or a 1 cm diameter porous graphite counter electrode. An Origalys (Rillieux-la-Pape, France) 3 M KCl Ag|AgCl reference electrode was used in all electrochemical experiments. All results were reported versus the reversable hydrogen electrode (RHE). A rotating ring disk working electrode was used, consisting of an edge plane pyrolytic graphite disk and a platinum ring, mounted in Teflon and rotated using a MSR rotator (Pine Instruments, Durham, NC, USA). The disk was renewed before modification with 1200 grit emery paper. The electrode surface was modified according to previously used protocols [20,26]. In short, a 1:1 ratio mixture of CNT and OCNFePc was dispersed in a 3:1 solution of isopropanol-water with 30 min of sonication. 20 μL of this mixture was then deposited on the graphite surface in four 5 μL aliquots with drying under nitrogen flow followed by 2 μL of Nafion™ solution followed by drying under nitrogen. Electrochemical measurements were performed using an Autolab PGSTAT 302 N with a dual mode bipotentiostat module. The ring potential was set to 1.56 V or 1.25 V for pH 13 and pH 1 buffer respectively. The buffer was saturated with nitrogen gas for cyclic voltammetry and oxygen for linear sweeps. Buffer solutions were changed at least daily to avoid possible contamination effecting the results. Background currents were subtracted.

All spectroscopic analysis was conducted on dried samples. Fourier Transform infrared spectroscopy (FTIR) analysis was conducted using a Bruker Alpha FTIR with ATR accessory. EPR spectra were conducted on powder samples at 298 K with a Bruker EMX-1572 spectrometer working at ~9.39 GHz (X-band). XPS measurements were carried out at the school of Chemistry, Nottingham University, on powder samples using a Kratos AXIS Ultra DLD instrument under a vacuum better than $5*10^{-9}$ Torr with wide energy range survey collected at pass energy of 80 eV in hybrid slot lens mode and a step size of 0.5 eV. High resolution XPS data on the C 1s, N 1s, and F 2p photoelectron peaks were collected at pass energy 20 eV with collection times of 5 min. The X-ray source was a monochromated Al Ka radiation run at 120 W. Spin-polarized density functional theory (DFT) calculations were performed with the Quantum-ESPRESSO ab initio package using methods previously described [20,26,34–37]. The dispersive (π-π stacking) interaction of OCNFePc onto the CNT was included through the van der Waals exchange–correlation functional (vdW-DF2) [35]. Kohn–Sham eigenfunctions were expanded on a plane-waves basis set where the interaction between valence electrons and ion cores are described by ultrasoft pseudo-potentials [37]. Converged results have been achieved by using a cut-off energy of 35 Ry on plane waves and of 280 Ry on the electronic density. Carbon nanotubes of 288 atoms with a diameter of 11 Å were simulated in a large unit cell with periodic boundary conditions along the CNT axis. Molecular electrostatic potential was calculated for the optimized molecular geometry of OCNFePc in its oxidation state of + 2 and triplet state at the same level of theory of the optimization, B3LYP/6-31G(d,p), by using the package Gaussian 09 [38].

3. Results and discussion.

3.1. Spectroscopic characterization

EPR spectra of OCNFePc and OCNFePc-CNT powders at 298 K were recorded (Fig. 1(A)). In both cases, an EPR signal was observed due to the odd spin of the metallic center of the phthalocyanine. An intense signal was observed for the OCNFePc with a lower G factor (2.01417) than for OCNFePc-CNT (2.07803). This last result correlates well with recently published results (2.06909) [20]. This higher value compared to free OCNFePc may be explained by high spin delocalization to the CNT matrix and its higher hydrophobic character [39]. The broadening signal in the presence of CNTs is related to the longer relaxation lifetime [40] particularly with the spin-net which is provided by non-covalent interactions with the π-electrons of the CNT (Fig. 1(A)) [20].

The FTIR spectra of OCNFePc and OCNFePc-CNT are shown (Fig. 1(B)). Analysis of the composites demonstrate the presence of OCNFePc with the nanotubes.

Wide-scan XPS was performed on the OCNFePc and OCNFePc-CNT powder samples (Fig. 1(C)). Both spectra were similar in that the N 1s peak agree with literature values [32]. Moreover, high-resolution Fe 2p core-level spectra (Fig. 1(C) inset) show the Fe $2p_{3/2}$ value for OCNFePc-CNT was higher than OCNFePc, partially explaining the enhanced ORR performance of OCNFePc bound to CNTs. The corresponding shift of the Fe $2p_{3/2}$ spectrum to higher binding energies is similar to that shown by Fe^{3+} species, suggesting a more positive electron density. The C 1s and O 1s peaks observed exhibit higher concentrations of carbon and oxygen for OCNFePc-CNT than OCNFePc.

3.2. Electrochemical characterization.

Cyclic voltammetry was conducted for the composite in 0.1 M NaOH (pH 13) and 0.1 M H_2SO_4 (pH 1) solutions (Fig. 2 (A) and (B)). The peaks of the redox couples (i.e. the Fe(III)/(II) and the Fe(II)/(I)) are not very well defined which would suggest low concentrations of OCNFePc but integration of the redox peak reveals concentration in the order of approximately 7×10^{-10} mol cm^{-2} (detailed results are summarized in Table 1) which agrees well with previous results obtained in the presence of CNT][13]. Stronger currents are visible at pH 1. Those differences have been reported to be caused by different protonation states of the phthalocyanine [41]. The Fe(II)/(I) redox transition occurs at approx. 0.30 V at pH 13 and 0.18 V vs RHE at pH 1 and the Fe(III)/(II) transition occurs at approx. 0.87 V at pH 13 and 0.70 V at pH 1. For the Fe(III)/Fe(II) redox couple of previously studied FeN4-CNT, values of 0.83 for the unsubstituted Fe phthalocyanine (FePc), 0.92 V for Fe hexadecachlorophthalocyanine (16(Cl)FePc) [13] and 0.99 V for the Fe hexadecafluorophthalocyanine (16(F)FePc) [20], at pH 13 have been reported (Table 1).

Linear sweeps (Fig. 2 (C) and (D)) show strong differences in the ORR activity in the two buffers. The onset voltage was 0.95 V at pH 13 and 0.79 V at pH 1. In pH 13 close to four e^- are transferred while in pH 1 around 3 e^- are transferred indicating only partial ORR. Further evidence for the increased production of H_2O_2 in acid medium was provided by the Pt ring electrode which showed over ten times the current at pH 1 as pH 13 (Fig. 2 (E) and (F)). Tafel plots for each buffer was -0.05 V $decade^{-1}$ at pH 13 and -0.07 V $decade^{-1}$ at pH 1. The pH 1 value indicates a fast electron transfer followed by a rate-determining chemical step. The pH 13 value involves a fast one-electron transfer followed by a second slow one-electron transfer [20]. This difference in performance at different pH values has been reported [42].

In general, the electrochemical values given for these materials compare well with similar materials reported in the literature. The electron number at pH 13 compares very well with that of 16(F)FePc-CNT, 16(Cl)FePc-CNT, FePc-CNT and 4β(SO_3^-)FePc-CNT [13,20]. The turn over frequency (TOF) was estimated from the coverage of the electrode Γ and the kinetic current densities at the half wave potential of the ORR polarization curve, with values for OCNFePc-CNT at pH 13, of 1.2 s^{-1}. This value is lower than the values determined for 16(F)FePc-CNT and 16(Cl)FePc-CNT [20] indicating a greater rate of turnover for halogenated phthalocyanines compared to OCNFePc (Table 1). The results obtained with OCNFePc-CNT are promising and indicating similar activities as when in the presence of halogenated phthalocyanines. Even better results could be obtained through the study of OCNFePc in combination with other forms of nanoscale carbon materials as in [7,43]. Also OCNFePc-CNT was stable for at least 50 consecutives cycles at 5 mV/s in both buffers. The electrochemical results for OCNFePc-CNT in comparison with other electrocatalysts from previous reports [13,20] are summarized in Table 1.

3.3. Computational analysis

3.3.1. Computational analysis of OCNFePc, OCNFePc on CNT and O_2 binding on OCNFePc-CNT

The equilibrium geometry of OCNFePc shows a planar structure (Fig. 3 (A)), which can exist in three-spin configuration: singlet, triplet, and quintuplet (m = 0, 2, 4 μ_B respectively). The ground state is triplet (m = 2 μ_B), preserving FePc spin characteristics. For the singlet and triplet configuration, a difference in Fe-N_1 distance was observed. The interaction of the OCNFePc molecule adsorbed on a metallic single-walled CNT with 11 Å diameter was studied. Periodic boundary conditions were applied along the CNT axis. As a result, an infinite CNT with adsorbed molecules separated by 4.7 Å was simulated. The molecule was noted to be physisorbed on the CNT surface with a binding energy of −2.923 eV, adopting the curvature of the CNT (Fig. 3 (B)). For comparison, the binding energy of FePc is of −1.71 eV (the CN substituent of OCNFePc appears to increase its adsorption energy on the CNT). The distance between the Fe atom of OCNFePc and the CNT surface was determined to be 3.4 Å. The system is stable in three spin states, with a magnetic moment of m = 0, 2, 4 μ_B where the ground state is triplet (m = 2). The spin of OCNFePc does not change after adsorption onto a CNT. A binding energy for OCNFePc of −4.53 eV was determined for graphene, suggesting that on larger CNTs the OCNFePc adsorption energy increases.

The interaction of the O_2 molecules with the Fe atom of the OCNFePc-CNT complex was simulated. It was found that the adduct was stable in three spin configurations. The lowest energy system is singlet but very close in energy to the triplet state, suggesting both states can coexist. The O_2 binding energy was found to be −0.6 eV, which decreases for higher magnetic moments. The O_2 molecule adopts an end-on configuration, with one O atom bound to the Fe with a Fe-O-O angle of 119.3° for the stable spin state (m = 0) (Fig. 3 (C)). All the results are resumed in Table 2. For comparison, the O_2 binding energy on the FePc-CNT complex was found to be −0.70 eV (0.1 eV higher with respect to OCNFePc). These results may explain the better ORR activity of OCNPcFe-CNT as compared to FePc-CNT. For OCNPcFe adsorbed on graphene, the O_2 binding energy was found to be −0.61 eV, and it may be concluded that the size of the CNT has a small effect in the O_2 binding energy on the OCNPcFe-CNT complex and in the ORR activity.

3.3.2. Computational analysis of O_2 dissociation when adsorbed on OCNFePc-CNT

The minimum energy path for the O_2 dissociation after the interaction with the Fe center of OCNFePc-CNT was obtained by the nudged elastic band (NEB) method [37], using ten images along the reaction coordinates. An energy barrier of 1.36 eV for O_2 dissociation was calculated, as shown in the saddle point, the O_2 molecule binds with both Fe and C atoms (Fig. 3 (D)), showing that the dissociation occurs on the surface of the OCNFePc-CNT catalyst, as observed in other FePc-CNT systems [14–22].

To investigate the effect of the cyano residues on the charge density

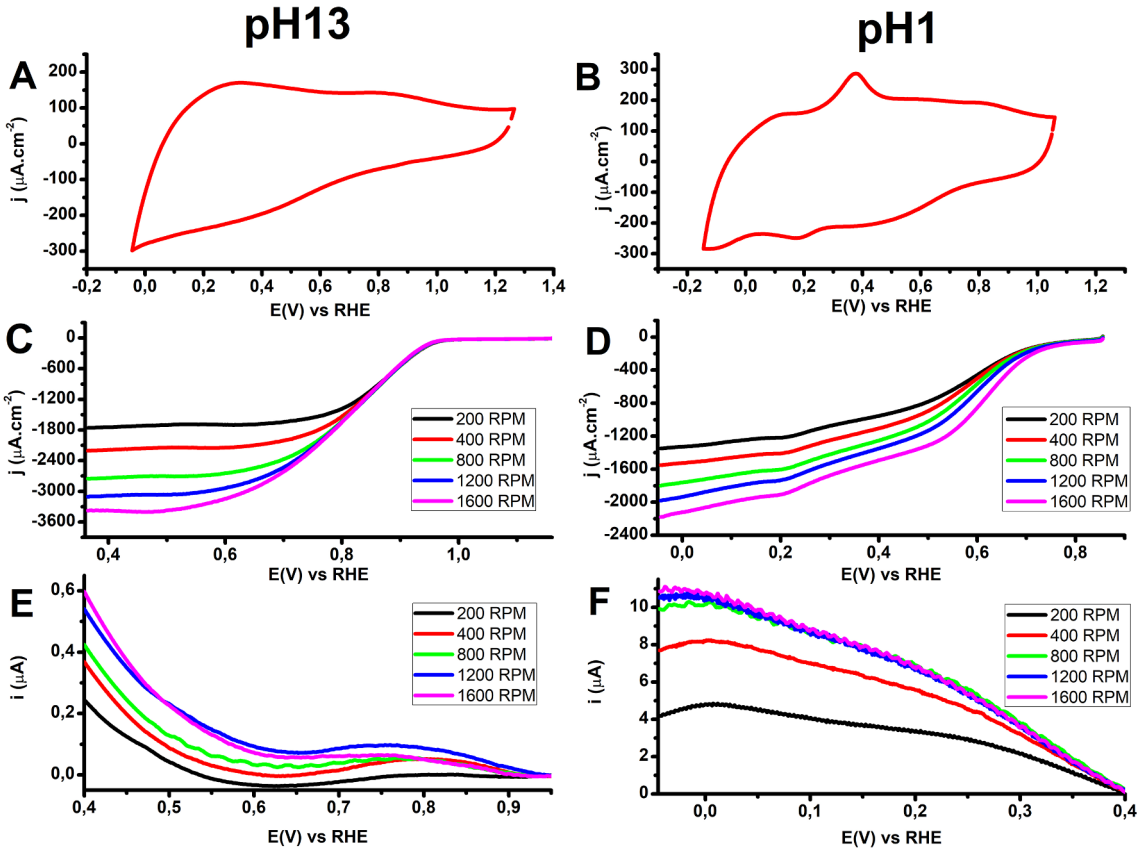

Fig. 2. Electrochemical analysis of OCNFeP-CNT showing cyclic voltammetry (A and C), linear sweeps (B and D) and platinum Ring electrode (E and F) measurements were performed in pH 13 (A, C and E) and pH 1 (B, D and F) buffers.

Table 1
Electrochemical characterization of electrodes modified with OCNFePc-CNT obtained in NaOH 0.1 M (pH 13) and H_2SO_4 0.1 M (pH 1). Electrochemical data from previous work [13,20] has been included for comparison.

Electrode material (pH)	n° e^-	Tafel (V)	E_{onset} (V vs. RHE)	$E_{Fe(II)/(I)}$ (V vs. RHE)	$E_{Fe(III)/(II)}$ (V vs. RHE)	Γ (mol*cm^{-2})	$TOF_{@(hw)}$ (s^{-1})
OCNFePc-CNT (pH13) this work	3.8	0.05	0.95	0.30	0.87	6.3×10^{-10}	1.2
OCNFePc-CNT (pH1) this work	3.1	0.07	0.79	0.18	0.70	8.5×10^{-10}	0.7
16(F)FePc-CNT (pH1) reference [20]	3.5	0.07	0.81	0.61	0.75	2.7×10^{-9}	3.4
16(F)FePc-CNT (pH13) reference [20]	4.1	0.05	1.06	0.75	0.99	1.2×10^{-9}	5.4
16(Cl)FePc-CNT (pH13) reference [13]	4.1	0.04	0.97	/	0.92	7.6×10^{-10}	/
4β(SO_3)FePc-CNT (pH13) reference [13]	4.2	0.04	0.93	/	0.88	5.9×10^{-10}	/
FePc-CNT (pH13) reference [13]	3.9	0.04	0.92	/	0.83	7.9×10^{-10}	/

of the macrocycle, the molecular electrostatic potential of OCNFePc and FePc was calculated in the triplet state (Fig. 4). This was obtained in the geometry optimized at the same level of theory (B3LYP/6-31G(d,p)). By comparing with non-substituted FePc (Fig. 4 (A)), the cyano residue in OCNFePc provokes a decrease of charge density in the central core where the metal atom is localized, represented by a larger blue zone (Fig. 4 (B)). The aza nitrogen atoms and benzene rings change to more positive regions (cyan) in OCNFePc compared to FePc, and the cyano groups show negative (yellow) MEP values. These results demonstrate that the cyano residues act as electron-withdrawing moieties in OCNFePc. We also investigate the MEP of OCNFePc in other electronic states; singlet and quintuplet, and the results are shown in Fig. 4(C) and 4(D), respectively. The singlet state shows a drastic reduction of the more positive region in the core of phthalocyanine, which is rather localized on the metal (Fig. 5). The quintuplet state looks very similar to the triplet state. Spin density is also calculated for the open shell configurations and shown in Fig. 5(B) and 5(C) for the triplet and quintuplet states, respectively. Both figures indicate that the unpaired electrons are mainly localized on the core of the macrocycle and on the metal that would favor the oxygen reduction.

3.4. Formation of volcano correlation

The search of reactivity descriptors that would allow for *a priori* design of better catalysts has always been a challenge [12]. Using the extended Koutecky-Levich equation [$i_k = i_l*i/(i-i_l)$] after subtracting the capacitive current for the linear sweep during ORR at 1200 RPM in alkaline media and the calculated E_b, for OCNFePc-CNT, and using previously reported extractions for other MN4 [12,13,20] we draw a volcano plot where the log *i* for the studied complex was determined to be −0.14, positioning the complex next to the most active perfluorinated Fe phthalocyanine (16FFePc-CNT) and confirming the high activity of the complex and high electron withdrawing capacity of the CN residues (Graphical Abstract).

4. Conclusions

OCNFePc were characterized through a series of analysis techniques

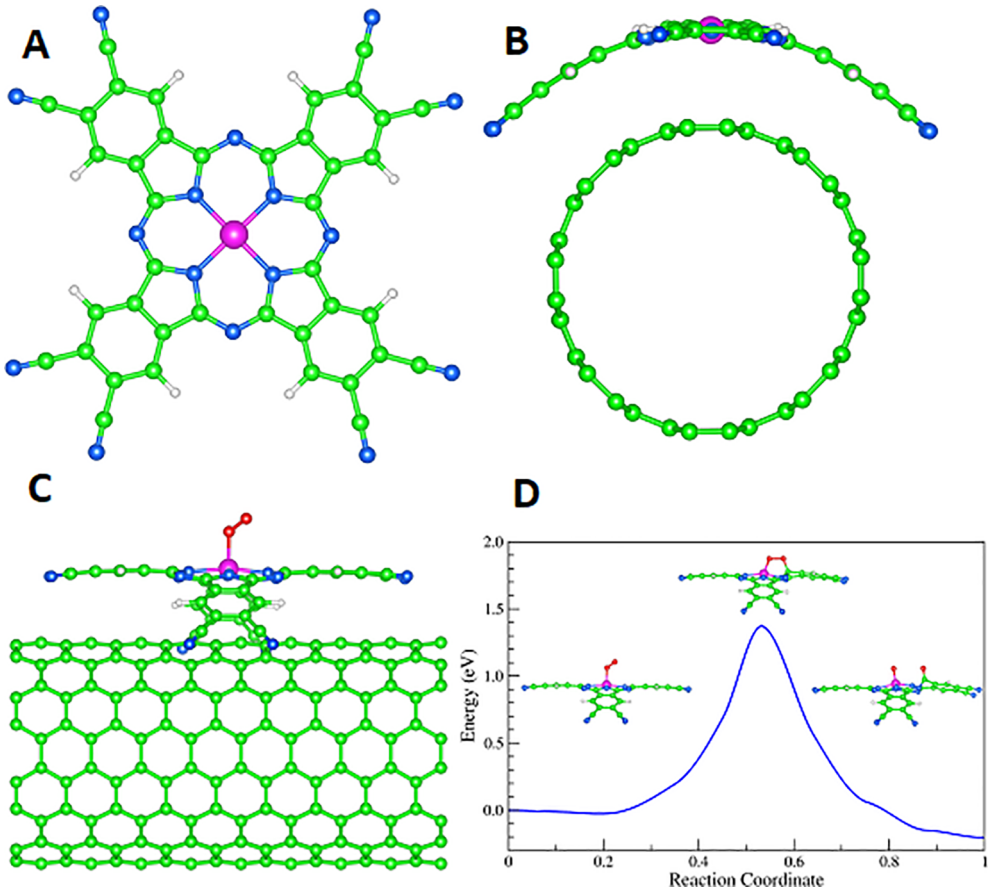

Fig. 3. Images from simulations of the interaction of OCNFePc with a single-walled carbon nanotube showing the structure of the OCNFePc molecule (A), it bound to a carbon nanotube (B), bound to a carbon nanotube with a dioxygen molecule bound to the Fe metal center (C) and the minimum energy profile for the dissociation of oxygen on the OCNFePc-CNT catalyst (D).

Table 2
OCNFePc in the allowed spin states (m (μ_B)): total energy (E_{total}), and equilibrium distance (d) of Fe in respect to N1 or N2. OCNFePc adsorbed on a CNT (OCNFePc-CNT) in the allowed spin states: total energy (E_{total}), binding energy (E_{bind}) and equilibrium distance (d) of OCNFePc to CNT. O_2 adsorbed on the Fe atom of OCNFePc-CNT in the allowed spin states: total energy (E_{total}), binding energy (E_{bind}) and bond distance (d) for O_2 adsorbed on the Fe atom. E_0 is the ground state energy.

m (μ_B)	$E_{total(OCNFePc)}$ (eV)	$d_{(Fe-N1)}$(Å)	$d_{(Fe-N2)}$ (Å)	$E_{total(OCNFePc-CNT)}$ (eV)	$E_{bind(OCNFePc-CNT)}$ (eV)	$d_{(OCNFePc-CNT)}$ (Å)	$E_{total(O2-OCNFePc-CNT)}$ (eV)	$E_{bind(O2)}$ (eV)	$d_{(Fe-O)}$ (Å)	$Angle_{(Fe-O-O)}$ (deg)
0	E_0 + 0.277	1.94	3.396	E_0 + 0.230	−2.693	3.396	E_0	−0.597	1.836	119.3
2	E_0	1.947	3.400	E_0	−2.923	3.401	E_0 + 0.040	−0.557	1.894	118.7
4	E_0 + 0.619	1.955	3.410	E_0 + 0.193	−2.730	3.402	E_0 + 0.179	−0.418	2.102	117.6

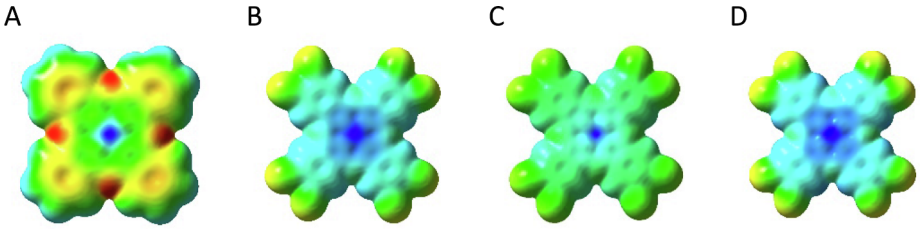

Fig. 4. Molecular electrostatic potential (MEP) mapped into the charge density isosurface of 0.0004 e/bohr3 calculated for (A) FePc and (B) OCNFePc as triplet state, (C) OCNFePc as singlet state and (D) OCNFePc as quintuplet state. Color scale red and yellow colors represent negative values, green, cyan and blue colors, positive. Red and blue represent extreme values. (For interpretation of the references to color in this figure legend, the reader is referred to the web version of this article.)

(FTIR, EPR and XPS) and through the examination for the ORR. At pH 13, 3.8 electrons were transferred indicating full reduction of oxygen to water while at pH 1, 3.1 electrons, which indicates only partial reduction to H_2O_2. The electrochemical values for these materials compare well with halogenated phthalocyanines such as 16(F)FePc. In all, the Log *i* value of this material at 0.760 V vs RHE is −0.14. Computational analysis shows that the OCNFePc attaches along the curve of the carbon nanotube bound through π–π stacking. The cyano residues act as electron-withdrawing moieties provoking a decrease in charge density around the central core where the metal atom is localized. The O_2-Fe binding energy value is −0.59 eV. This value is close to the value reported before for the apex of the volcano for fluorinated phthalocyanines (Graphical Abstract). Changing the ligands in the phthalocyanine molecule the activity and therefore the position of a given molecule on a volcano correlation can be controlled. It is interesting that more active complexes exhibit Fe(III)/(II) redox couples which approach the reversible potential of the ORR.

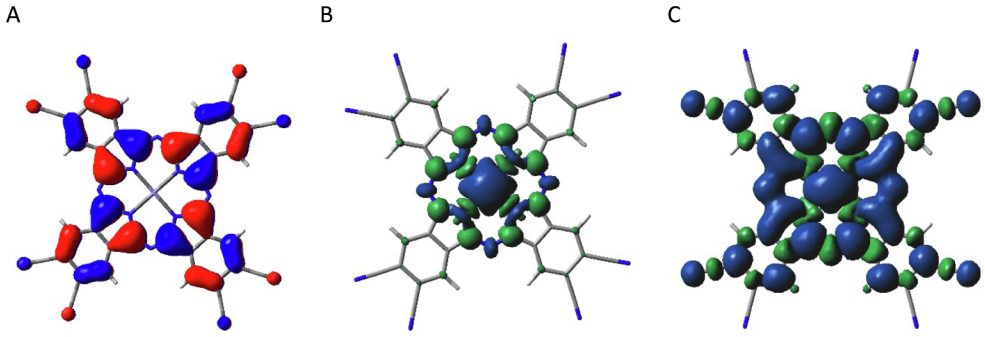

Fig. 5. Surfaces of HOMO molecular orbital for singlet state (A), spin densities for triplet state (B) and quintuplet state (C) calculated for OCNFePc considering Fe(II) in all cases.

Declaration of Competing Interest

The authors declare that they have no known competing financial interests or personal relationships that could have appeared to influence the work reported in this paper.

Acknowledgements

The authors thank FONDECYT project numbers: 1181037, 1181840, 11170879, 1170480, 1171719, the laboratory of free radicals for use of the EPR (USACH, CONICYT-FONDEQUIP EQM140060), CEDENNA AFB180001 and DICYT POSTDOC 021541AV and 021942T. J.H.Z thanks Millenium RC120001, Project Anillo ACT 192175.

References

[1] J.H. Zagal, S. Griveau, J.F. Silva, T. Nyokong, F. Bedioui, Coord. Chem. Rev. 254 (2010) 2755–2791.
[2] A.B. Sorokin, Chem. Rev. 113 (2013) 8152–8191.
[3] H. Lu, N. Kobayashi, Chem. Rev. 116 (2016) 6184–6261.
[4] Y.-M. Zhao, G.-Q. Yu, F.-F. Wang, P.-J. Wei, J.-G. Liu, Chem – A Eur. J. 25 (2019) 3726–3739.
[5] R. Jasinski, Nature 201 (1964) 1212–1213.
[6] T. Sun, B. Tian, J. Lu, C. Su, J. Mater. Chem. A 5 (2017) 18933–18950.
[7] J. Yang, F. Toshimitsu, Z. Yang, T. Fujigaya, N. Nakashima, J. Mater. Chem. A 5 (2017) 1184–1191.
[8] K. Kumar, P. Gairola, M. Lions, N. Ranjbar-Sahraie, M. Mermoux, L. Dubau, A. Zitolo, F. Jaouen, F. Maillard, ACS Catal. 8 (2018) 11264–11276, https://doi.org/10.1021/acscatal.8b02934.
[9] N. Ramaswamy, U. Tylus, Q. Jia, S. Mukerjee, J. Am. Chem. Soc. 135 (2013) 15443–15449.
[10] A.A. Gewirth, J.A. Varnell, A.M. DiAscro, Chem. Rev. 118 (2018) 2313–2339.
[11] M.J. Workman, A. Serov, L. Tsui, P. Atanassov, K. Artyushkova, ACS Energy Lett. 2 (2017) 1489–1493.
[12] J.H. Zagal, M.T.M. Koper, Angew. Chem. Int. Ed. 55 (2016) 14510–14521.
[13] R. Venegas, F.J. Recio, C. Zuñiga, M. Viera, M.-P. Oyarzún, N. Silva, K. Neira, J.F. Marco, J.H. Zagal, F. Tasca, PCCP 19 (2017) 20441–20450.
[14] C. Linares-Flores, J. Espinoza-Vergara, J.H. Zagal, R. Arratia-Pérez, Chem. Phys. Lett. 614 (2014) 176–180.
[15] J. Masa, K. Ozoemena, W. Schuhmann, J.H. Zagal, J. Porphyr. Phthalocyan. 16 (2012) 761–784.
[16] J.H. Zagal, F. Javier Recio, C.A. Gutierrez, C. Zuñiga, M.A. Páez, C.A. Caro, Electrochem. Commun. 41 (2014) 24–26.
[17] A. Kumar, Y. Zhang, W. Liu, X. Sun, Coord. Chem. Rev. 402 (2020) 213047.
[18] M.T.M. Koper, J. Electroanal. Chem. 660 (2011) 254–260.
[19] P. Cañete, J.F. Silva, J.H. Zagal, J. Chil. Chem. Soc. 59 (2014) 2529–2530.
[20] G. Abarca, M. Viera, C. Aliaga, J.F. Marco, W. Orellana, J.H. Zagal, F. Tasca, J. Mater. Chem. A 7 (2019) 24776–24783.
[21] R. Venegas, F.J. Recio, J. Riquelme, K. Neira, J.F. Marco, I. Ponce, J.H. Zagal, F. Tasca, J. Mater. Chem. A 5 (2017) 12054–12059.
[22] A. Pizarro, G. Abarca, C. Gutiérrez-Cerón, D. Cortés-Arriagada, F. Bernardi, C. Berrios, J.F. Silva, M.C. Rezende, J.H. Zagal, R. Oñate, I. Ponce, ACS Catal. 8 (2018) 8406–8419.
[23] J. Govan, W. Orellana, J.H. Zagal, F. Tasca, J. Solid State Electrochem. (2020), https://doi.org/10.1007/s10008-019-04489-x.
[24] F. Tasca, F.J. Recio, R. Venegas, D.A. Geraldo, M. Sancy, J.H. Zagal, Electrochim. Acta 140 (2014) 314–319.
[25] J. Riquelme, K. Neira, J.F. Marco, P. Hermosilla-Ibáñez, W. Orellana, J.H. Zagal, F. Tasca, Electrochim. Acta 265 (2018) 547–555.
[26] M. Viera, J. Riquelme, C. Aliaga, J.F. Marco, W. Orellana, J.H. Zagal, F. Tasca, Front. Chem. 8 (2020) 22.
[27] C. Hansch, A. Leo, R.W. Taft, Chem. Rev. 91 (1991) 165–195.
[28] F. Bedioui, S. Griveau, T. Nyokong, A. John Appleby, C.A. Caro, M. Gulppi, G. Ochoa, J.H. Zagal, PCCP 9 (2007) 3383–3396.
[29] C. Linares-Flores, F. Mendizabal, R. Arratia-Pérez, N. Inostroza, C. Orellana, Chem. Phys. Lett. 639 (2015) 172–177.
[30] J.H. Zagal, G.I. Cárdenas-Jirón, J. Electroanal. Chem. 489 (2000) 96–100.
[31] S.-J. Kim, M. Matsumoto, K. Shigehara, J. Porphyr. Phthalocyan. 04 (2000) 136–144.
[32] Z. Honda, Y. Sakaguchi, M. Tashiro, M. Hagiwara, T. Kida, M. Sakai, T. Fukuda, N. Kamata, Appl. Phys. Lett. 110 (2017) 133101.
[33] H. Zhong, K.H. Ly, M. Wang, Y. Krupskaya, X. Han, J. Zhang, J. Zhang, V. Kataev, B. Büchner, I.M. Weidinger, S. Kaskel, P. Liu, M. Chen, R. Dong, X. Feng, Angew. Chem. 58 (2019) 10677–10682.
[34] P. Giannozzi, S. Baroni, N. Bonini, M. Calandra, R. Car, C. Cavazzoni, D. Ceresoli, G.L. Chiarotti, M. Cococcioni, I. Dabo, A. Dal Corso, S. de Gironcoli, S. Fabris, G. Fratesi, R. Gebauer, U. Gerstmann, C. Gougoussis, A. Kokalj, M. Lazzeri, L. Martin-Samos, N. Marzari, F. Mauri, R. Mazzarello, S. Paolini, A. Pasquarello, L. Paulatto, C. Sbraccia, S. Scandolo, G. Sclauzero, A.P. Seitsonen, A. Smogunov, P. Umari, R.M. Wentzcovitch, J. Phys.: Condens. Matter 21 (2009) 395502.
[35] K. Lee, É.D. Murray, L. Kong, B.I. Lundqvist, D.C. Langreth, Phys. Rev. B 82 (2010) 81101.
[36] K.F. Garrity, J.W. Bennett, K.M. Rabe, D. Vanderbilt, Comput. Mater. Sci. 81 (2014) 446–452.
[37] G. Henkelman, B.P. Uberuaga, H. Jónsson, J. Chem. Phys. 113 (2000) 9901–9904.
[38] Frisch MJ, Trucks GW, Schlegel HB, Scuseria GE, Robb MA, Cheeseman JR, Scalmani G, Barone V, Mennucci B, Petersson GA, Nakatsuji H, Caricato M, Li X, Hratchian HP, Izmaylov AF, Bloino J, Zheng G, Sonnenberg JL, Hada M, Ehara M, Toyota K, Fukuda R, Hasegawa J, Ishida M, Nakajima T, Honda Y, Kitao O, Nakai H, Vreven T, Montgomery JAJ, Peralta JE, Ogliaro F, Bearpark M, Heyd JJ, Brothers E, Kudin KN, Staroverov VN, Kobayashi R, Normand J, Raghavachari K, Rendell A, Burant JC, Iyengar SS, Tomasi J, Cossi M, Rega N, Millam JM, Klene M, Knox JE, Cross JB, Bakken V, Adamo C, Jaramillo J, Gomperts R, Stratmann RE, Yazyev O, Austin AJ, Cammi R, Pomelli C, Ochterski JW, Martin RL, Morokuma K, Zakrzewski VG, Voth GA, Salvador P, Dannenberg JJ, Dapprich S, Daniels AD, Farkas Ö, Foresman JB, Ortiz J V., Cioslowski J, Fox DJ (2009) Gaussian 09.
[39] C. Aliaga, P. Torres, F. Silva, Magn. Reson. Chem. 50 (2012) 779–783.
[40] J.A. Weil, J.R. Bolton, Electron Paramagnetic Resonance: Elementary Theory and Practical Applications, 2nd ed., John Wiley & Sons Ltd, New York, 2006.
[41] M.N. Golovin, P. Seymour, K. Jayaraj, Y.S. Fu, A.B.P. Lever, Inorg. Chem. 29 (1990) 1719–1727.
[42] J. Zagal, P. Bindra, E. Yeager, J. Electrochem. Soc. 127 (1980) 1506–1517.
[43] J. Yang, J. Tao, T. Isomura, H. Yanagi, I. Moriguchi, N. Nakashima, Carbon N Y 145 (2019) 565–571.